

## Article

# Data-Driven Insights into Population Exposure Risks: Towards Sustainable and Safe Urban Airspace Utilization by Unmanned Aerial Systems

Hongbo He <sup>1,2,3</sup> , Xiaohan Liao <sup>1,2,3,4</sup>, Huping Ye <sup>1,2,3,4,\*</sup> , Chenchen Xu <sup>1,3,4</sup>  and Huanyin Yue <sup>1,2,3,4</sup>

- <sup>1</sup> State Key Laboratory of Resources and Environment Information System, Institute of Geographic Sciences and Natural Resources Research, Chinese Academy of Sciences, Beijing 100101, China; hehb.20b@igsnr.ac.cn (H.H.); liaoxh@igsnr.ac.cn (X.L.); xucc.14s@igsnr.ac.cn (C.X.); yuehy@leris.ac.cn (H.Y.)
- <sup>2</sup> University of Chinese Academy of Sciences, Beijing 100049, China
- <sup>3</sup> Key Laboratory of Low Altitude Geographic Information and Air Route, Civil Aviation Administration of China, Beijing 100101, China
- <sup>4</sup> The Research Center for UAV Applications and Regulation, Chinese Academy of Sciences, Beijing 100101, China
- \* Correspondence: yehp@igsnr.ac.cn

**Abstract:** With the rapid increase in unmanned aerial vehicles (UAVs), ensuring the safety of airspace operations and promoting sustainable development of airspace systems have become paramount concerns. However, research dedicated to investigating the population exposure risks of UAV operations in urban areas and their spatial pattern is still missing. To address this gap, this study evenly divides the urban space into uniform grids and calculates critical areas for two UAV types within each grid. By integrating geospatial data, including buildings, land use, and population, data-driven risk maps are constructed to assess the spatial distribution patterns and potential population exposure risks of two UAV types and compare them with commonly used census units. The results indicate that the mean time between failures (MTBF) for the selected generic and rotary-type UAVs can be up to  $9.04 \times 10^8$  h and  $1.22 \times 10^8$  h, respectively, at acceptable risk levels, considering uncertainties. The spatial pattern of population exposure risk exhibits spatial heterogeneity and multi-scale effects in urban areas, aligning with population distribution. High-risk areas concentrate in regions characterized by high population mobility, such as transport hubs, commercial service areas, residential zones, and business districts. Additionally, the comparison emphasizes the potential bias introduced by using census units in risk assessment, especially in regions with significant urban build-up. This framework enables the evaluation of safety and acceptability across diverse urban land use areas and offers guidance for airspace management in megacities, ensuring the safe integration of UAVs in urban environments.

**Keywords:** unmanned aerial vehicle; risk assessment; risk map; population exposure risk; airspace management



**Citation:** He, H.; Liao, X.; Ye, H.; Xu, C.; Yue, H. Data-Driven Insights into Population Exposure Risks: Towards Sustainable and Safe Urban Airspace Utilization by Unmanned Aerial Systems. *Sustainability* **2023**, *15*, 12247. <https://doi.org/10.3390/su151612247>

Academic Editors: Honghai Zhang, Xinglong Wang, Gang Zhong and Xinpeng Zhu

Received: 11 July 2023

Revised: 31 July 2023

Accepted: 8 August 2023

Published: 10 August 2023



**Copyright:** © 2023 by the authors. Licensee MDPI, Basel, Switzerland. This article is an open access article distributed under the terms and conditions of the Creative Commons Attribution (CC BY) license (<https://creativecommons.org/licenses/by/4.0/>).

## 1. Introduction

Unmanned aerial vehicles (UAV) have been receiving significant attention due to their many commercial and civilian applications, including precise agriculture, terrain mapping [1], rescue, and delivery of foods or medical goods [2], among many others [3,4]. Unfortunately, the use of unmanned aerial systems (UAS) in urban areas is strongly restricted by regulations concerning unmanned operations in the civil airspace, primarily for safety reasons. The two critical safety hazards posed by UAVs operating in urban low-airspace environments are midair collision with another aircraft and discontinuance or breakdown of flight over a populated area [5]. The former risk (usually called air risk) is strongly related to the level of integration for UAS operations in the National Airspace System (NAS). Air

risk must be addressed through the appropriate certification of UAVs for operation over an urban area, combined with robust and comprehensive airspace structure design and air traffic management [6]. The latter risk to people and property on the ground due to the hazard of discontinuance or breakdown of flight (usually called ground risk) is the focus of this research. In this context, sustainable urban air traffic management is of paramount importance. However, urban areas are characterized as central core regions with dense population, high-value infrastructure, and a variety of associated socio-economic activities [7,8]. In addition, there are some technological difficulties, such as surveillance with and communication with UAVs in low-altitude airspace, especially in urban very low-level airspace [9]. Therefore, the complexity and uncertainty of urban environment operation affects the process of large-scale application of UAVs.

In the field of manned aviation, the assessment of risk has been a topic of study for several decades [10], and the population exposure risk (PER) is clearly defined as an equivalent level of safety (ELS). Current policy to enable the integration process of UAVs into the NAS is inspired by manned aviation [11]. ELS is calculated using the expected number of fatalities on the ground per flight hour given the UAS operation [12]. Most studies have used the ELS as a preliminary method for quantifying PER [13–15]. In particular, the Joint Authorities for Rulemaking on Unmanned Systems (JARUS) has proposed the Specific Operational Risk Assessment (SORA) [16], which is a novel classification evaluation framework that integrates air and ground risks and mitigation measures. Related studies have applied the SORA model to undertake applications in specific operational scenarios [17], but the ground risk classification criteria within the SORA model lack specific and detailed quantitative indicators, making it less generalizable. Therefore, in order to calculate ELS more scientifically and reasonably, various studies have proposed various population exposure risk models (PERM) [18]. These models mainly involve the combination of multiple sub-models, including the probability of failure, the type of failure [13], the crash area estimation [19], the protection of shelter (buildings, trees, etc.) [20], and the model of such a crash resulting in a fatality [21]. However, accurately quantifying ground risk is challenging due to the various factors that may impact the ELS, along with the associated uncertainties, such as aircraft type, flight area, mission type, population spatial distribution, weather conditions, etc. [22,23].

Risk maps, which incorporate risk assessment models and a Geographic Information System (GIS) to visualize potential risk, have been employed in various fields, including the identification and management of epidemic transmission risk, noise exposure risk, flood risk, and air pollution exposure risk. For complex systems like UASs, PER assessment approaches require considering all relevant factors associated with the geographical environment in order to more accurately quantify the vulnerability and resilience to different crash risks. However, few studies have utilized risk maps to quantify the PER of UAS operation. Primatesta [13] generated a risk map through a probabilistic approach using different UAV parameters, uncontrolled descent events, environmental characteristics, and uncertainties on parameters. Kim [24] generated a risk map to compute the third-party risk on the ground, which was used to determine the capacity of the corridor. Pang [25] computed an integrated risk cost mapping for different flight height layers and developed a cost-based path optimization model for reducing the risk cost. Risk maps show the spatial distribution of PER, which is convenient for the evaluation of UAS operations in specific scenarios [26]. To quantify population density, most previous studies used the uniform density value based on census data [20]. Although uniform data are simpler to get, they do not accurately reflect the population distribution at a finer spatio-temporal resolution [27]. Furthermore, the above studies did not further explore and analyze the risks from the perspective of functional urban areas. Specifically, each urban administrative/census unit consists of many components (e.g., buildings, streets, green space, and blue space), all of which show a great difference in spatial distribution and have significant impact on the quantification of risk. The geographical data examined in this study mainly comprise point or polygonal elements, such as building footprints, incident points, and impact areas,

which are typically modeled as vector elements. The spatial grid model represents a highly intuitive means to assess risk, facilitating visualization and quantification. Unlike a vector model, a spatial grid-based map can partition space into smaller cells, enabling a more detailed analysis of the spatial patterns of risk.

The applications of geospatial big data have gained tremendous popularity in recent years, thereby providing new opportunities to produce accurate gridded population and urban land use datasets at finer spatial resolutions [28,29]. Many high-quality population datasets have been produced and are available in finer spatial detail [30], such as Gridded Population of the World (GPW) [31], LandScan [32], and WorldPop [33]. To fill the deficiency of fine-scale urban PER analysis of UAV operations, this research utilized grid-based risk maps combined with the high resolution of population and land use details to (1) assess the ground impact of two types of UAVs, (2) explore the PER distribution pattern characteristics and reveal the high PER hotspot from the perspective of functional areas, and (3) explore the risk and disparities based on different spatial units. The framework of this study is shown in Figure 1. The research contributes to existing literature by expanding the application of multisource geospatial data in UAS risk assessment and management research, and its novelty is that it expands the literature by providing a high-resolution quantitative model to assess the exposure risk of UAV operations based on a combination of the GIS and ground risk models. The findings offer potential implications for urban air mobility management and facilitating the large-scale adoption of UAVs.

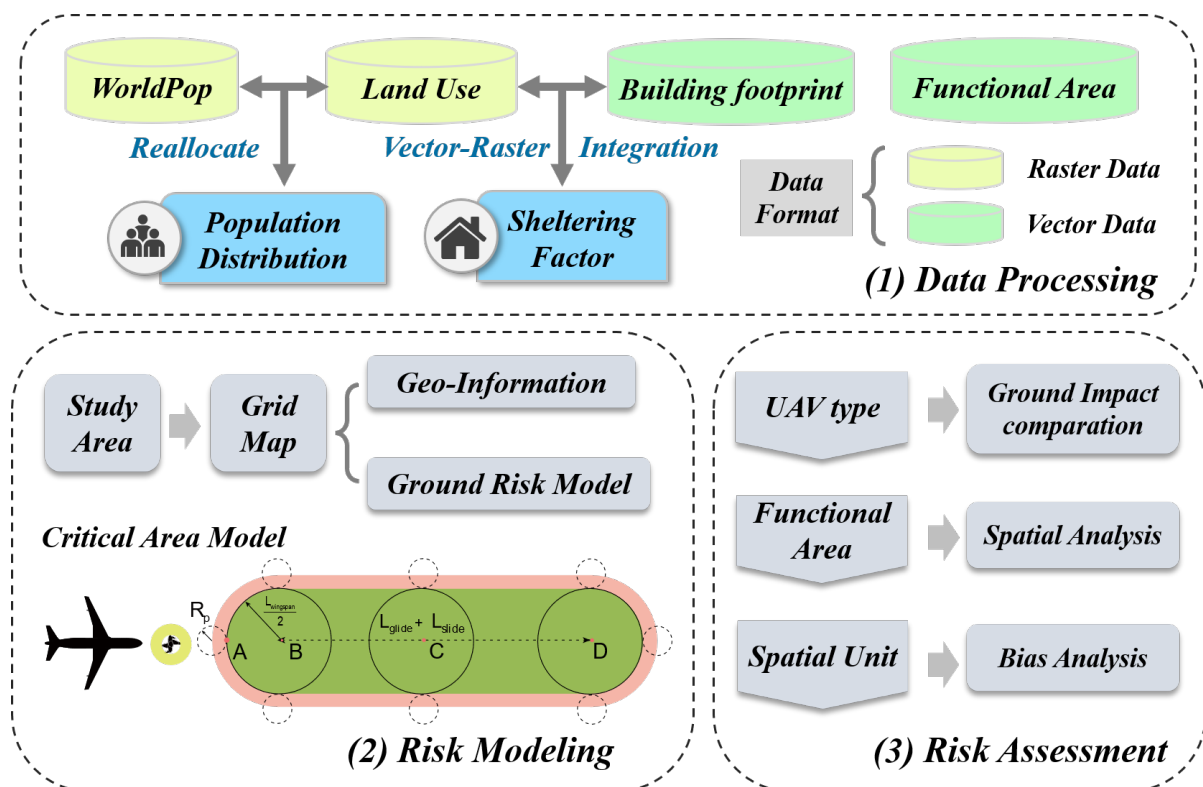


Figure 1. The framework of the study.

The structure of the paper is as follows: Section 2 introduces the study area, data preprocessing for model inputs and the population exposure risk model. Section 3 presents the results, which are subsequently discussed in Section 4. The paper concludes with a summary of the results and their implications for future research.

## 2. Materials and Methods

### 2.1. Study Area

Hangzhou, the provincial capital of Zhejiang, is a bustling metropolis in East China situated in the southern Yangtze River Delta and is well known as a major hub for e-commerce in China [34]. Its low average elevation provides advantageous conditions for the operation of UAS (Figure 2c, digital elevation model (DEM)). These favorable geographical features, combined with a well-established digital economy, provide a robust foundation for UAS operation. In recognition of these advantages, the Civil Aviation Administration of China has granted Hangzhou the first-ever specific unmanned aerial vehicle commissioning letter and unmanned aerial vehicle logistics distribution business license in China.

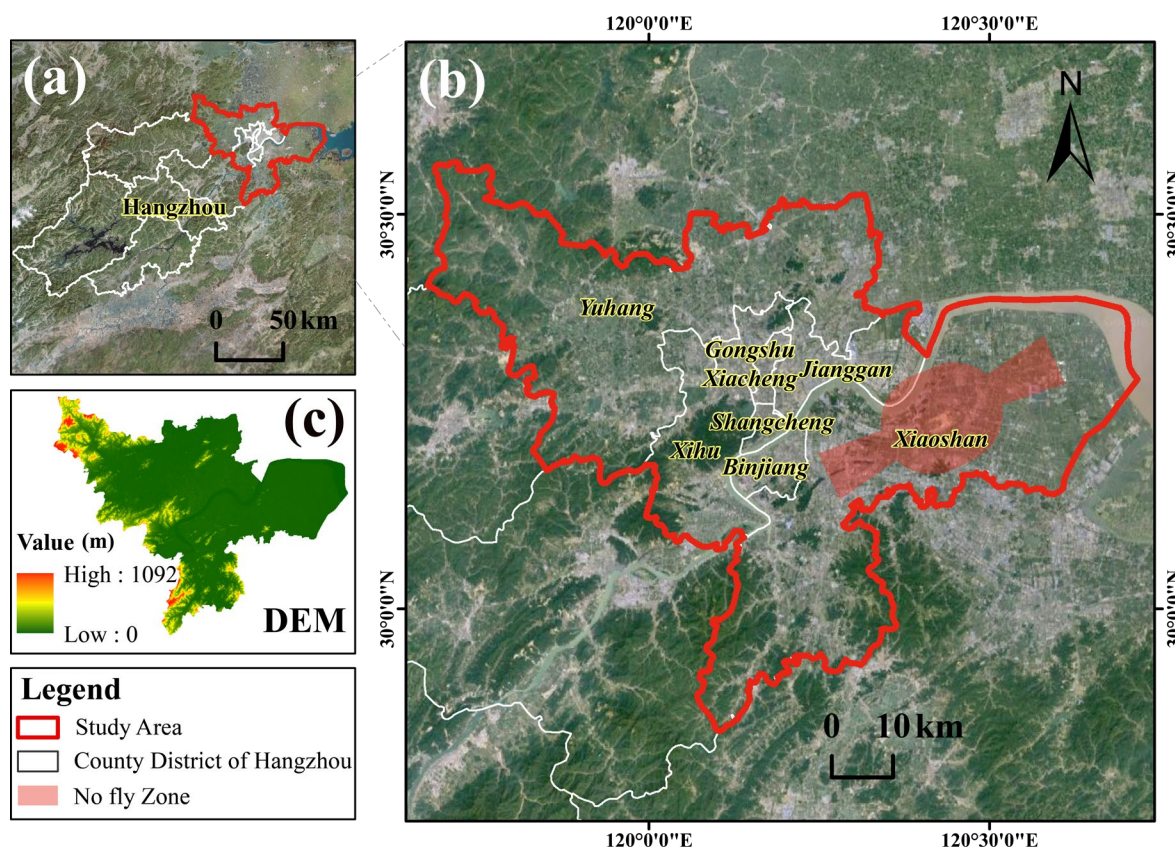


**Figure 2.** Location and environment of Hangzhou and study area. (a) Location of the study area (red-line boundary) in Hangzhou (white-line boundary). (b) Map of county administrative units in the study area, with no-fly zones as red polygons. (c) shows the elevation of the study area.

### 2.2. Generation of Population Exposure Risk Map

In our framework (shown in Figure 1), the risk map was created by dividing the study area into uniform cells and assigning a risk value to each cell. The cells correspond to geographic coordinates and various geographical attributes, such as population, shelter, and building footprints, were incorporated to capture the features of the area of interest. The generation of the PER map for low-altitude UAV operations involved combining the PERM with these geographical layers, as described in Sections 2.3.1 and 2.3.2.

#### 2.2.1. Geographical Data

**Population density layer:** In Figure 3, we present the population data of the study area at various scales. The census data (shown in Figure 3a) at the sub-district level were obtained from the Hangzhou Bureau of Statistics. Additionally, we present the population grid datasets: WorldPop (spatial resolution is 100 m, in Figure 3b, <https://hub.worldpop.org>).

org/, accessed on 20 July 2022). Since the horizontal distance of a small UAS crash is generally less than 100 m, this paper finally used the WorldPop dataset as the population density layer in order to inscribe a more accurate population exposure risk map.

**Sheltering layer:** When estimating the UAV fall impact of the people on the ground, it is necessary to consider the shelter effect associated with the land cover. To characterize the land cover types in each risk map unit, we used the 10 m Finer Resolution Observation and Monitoring of Global Land Cover (FROM-GLC) products [29]. Urban building geospatial data were obtained from OpenStreetMap (<https://www.openstreetmap.org> (accessed on 20 June 2020, shown in Figure 4d)).

**No-fly zone layer:** Most related study used the no-fly zone to help people identify areas where they cannot operate a UAV. No-fly zones are typically determined by national regulation agencies, nature-sensitive areas, security areas, airports restrictions, and temporary restrictions due to major sporting events [35]. In this study, we assumed that there was no temporary no-fly zone in the study area except for the clearance area of civil airports [9] (Figure 2b).

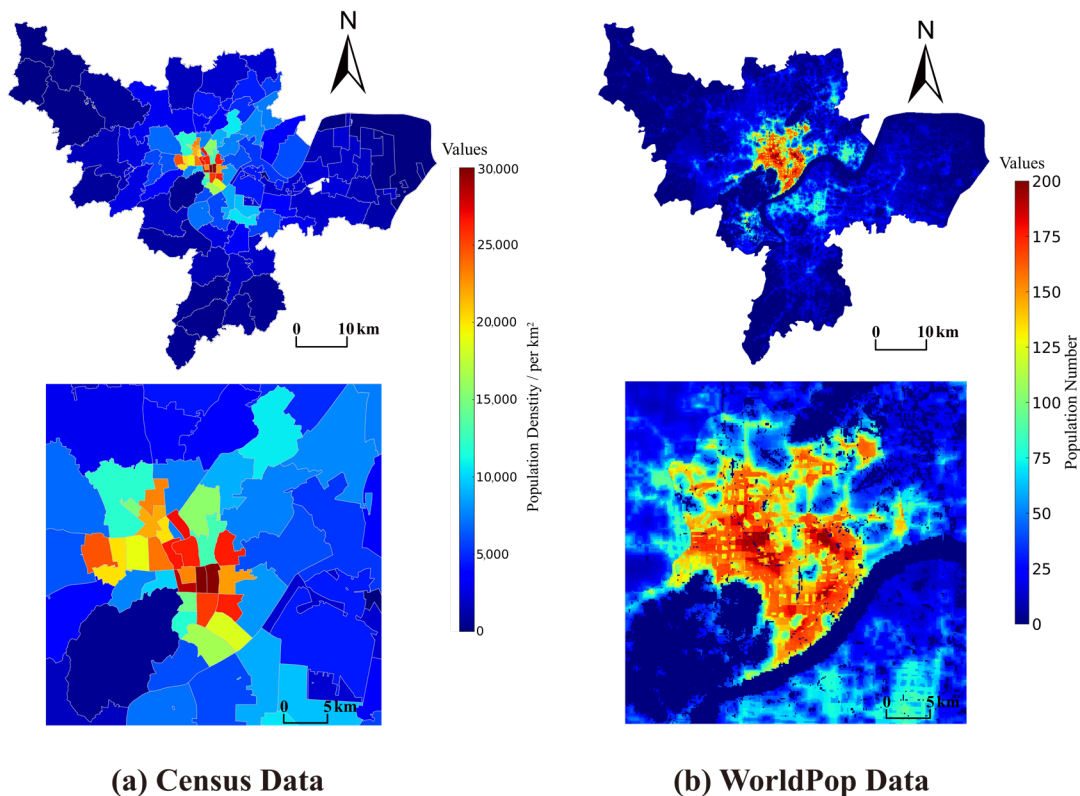


**Figure 3.** Spatial distribution of population at different scales in Hangzhou: (a) census data; (b) WorldPop data/100 m.

Because of their different sources and formats, all data were further processed by unification of the geographic reference using the WGS\_1984\_UTM\_Zone\_51N. In addition, the vector data from the input geographical data layer were rasterized and the raster size was unified to 100 m as the uniform resolution for the grid-based risk map.

### 2.2.2. Data Processing for Risk Analysis

In order to solve the problem mentioned in introduction and to estimate the population spatial distribution and shelter factor more accurately, it was necessary to combine and further process the high-resolution geographical data in Section 2.2.1. As the main land cover type in the study area (shown in Figure 4a), impervious surfaces are defined as artificial structures closely related to the population that contain building roofs, roads, and industrial areas, and the sheltering factor of these subareas varies significantly [28].

Therefore, in this study, impervious surfaces were further subdivided, as were building roofs with a high sheltering effect and other areas with high exposure risk (shown in Figure 4b). Therefore, to more accurately estimate the PER, based on related research [36], we allocated the population density distribution weight and sheltering factor (shown in Figure 4) according to the land cover area, which portrays the distribution of the population in different types of land cover within the risk map units and the corresponding sheltering factor.

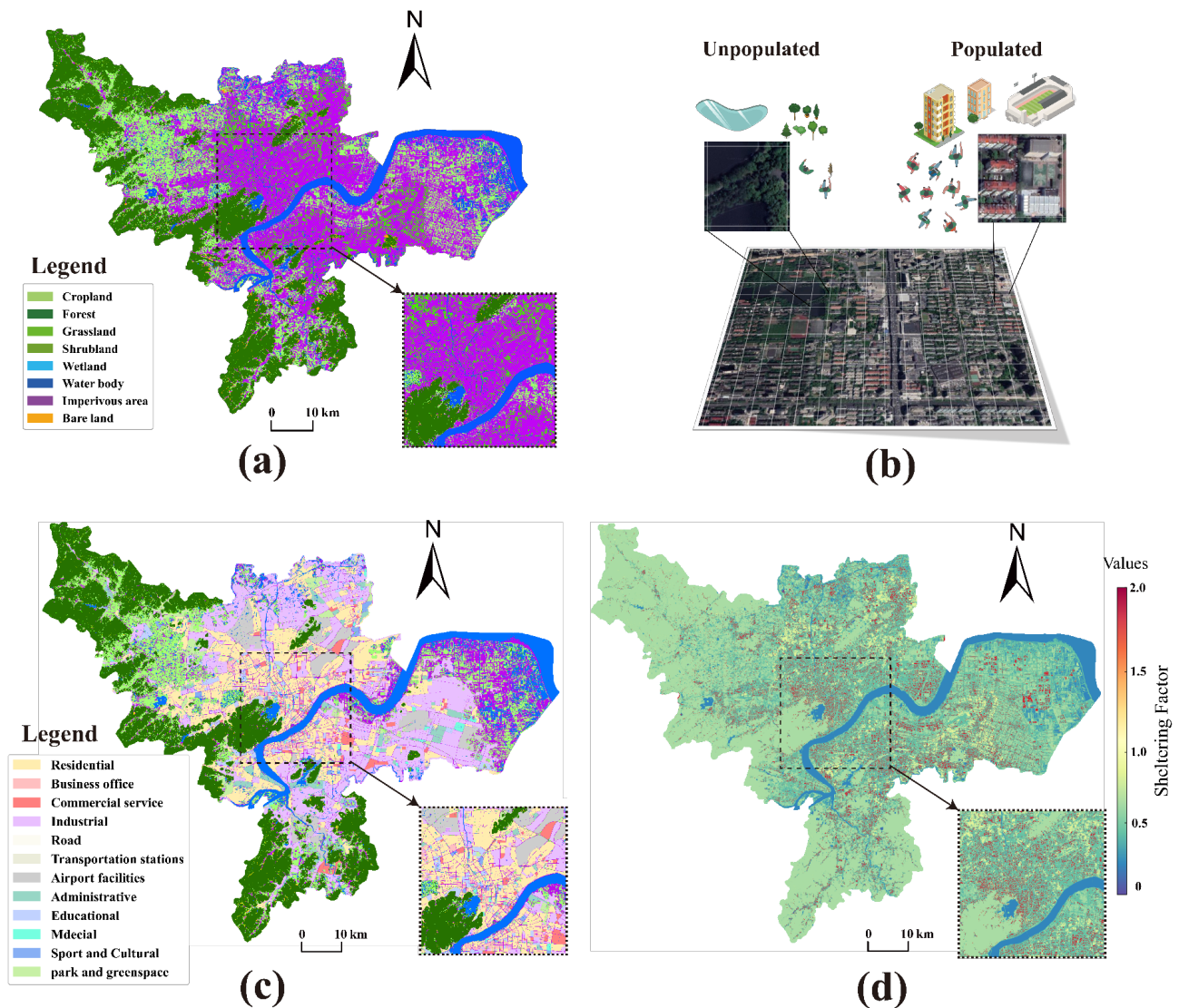


**Figure 4.** The input geographical data of population exposure risk. (a) Land cover data; (b) risk map grid comparison between populated and unpopulated area; (c) urban functional area; (d) sheltering factor map.

In order to cover the various types of UAVs available on the civil market that can be licensed for airworthiness in urban areas, we identified two different types of materials and configurations, defined as generic and rotary UAVs, respectively, in the present work, in terms of weights, dimensions, and configurations. The generic UAV (Zhihang V330, Shenzhen, China) selected for this study combines the superior aerodynamic performance of fixed-wing with the vertical take-off and landing function of multi-rotor, which can quickly take off and land vertically in complex geographical environments. A summary of the main configuration parameters of used UAVs is shown in Table 1. All of the data were

obtained from the official manual. The PERM (in Section 2.3) and experiments were then conducted accordingly with the two individual groups.

**Table 1.** Population density distribution weights and sheltering factors in different land cover types.

Land Cover Type	Population Density Weight <sup>1</sup>	Sheltering Factor <sup>1</sup>
Cropland	0.02	0.5
Forest	0.03	1.5
Grassland	0.02	0.5
Shrubland	0.02	0.8
Wetland	0.01	0.2
Water	0.02	0.2
Imperious area <sup>2</sup> —outdoor	0.3	0.3
Imperious area <sup>2</sup> —indoor	0.5	4
Bare land	0.03	0.2

<sup>1</sup> Population density weight and sheltering factor are both dimensionless quantities that participate in the computation of the model. <sup>2</sup> Imperious area is defined as artificial structures closely related to the population that contain building roofs, roads, and industrial areas.

### 2.3. Population Exposure Risk Model

For the purposes of this study, population exposure risk is defined as the likelihood that a particular type of UAV operating in a specific area poses a risk of injury or death to the people on the ground. The PER model for a UAV is based on a sequence of three conditional events: (1) the loss control of the UAV that leads to an uncontrolled crash on ground, (2) the total effective casualty area of the UAV body or fragment and the corresponding number of people affected, and (3) casualties caused by a crash on people after the shelter (building, tree, etc.) protection effect [5,11,13,20]. The probabilistic expectation of the serial combination of the three events describes the expected number of fatalities per hour of operation of the UAS [14], referred to as the expected safety level (ELS). For manned aircraft, the updated fatality rates based on National Transportation Safety Board (NTSB) data for the period of 1983 to 2006 are closer to  $10^{-7}$  per hour, including the fatalities after emergency landings, ditching, and other situations [11]. In order to achieve acceptance by the authorities or the public, most studies have used ELS for GRM that are an order of magnitude higher than those required for manned systems, at  $10^{-8}$  fatalities per hour [14,15]. Given that the estimation of failure probabilities is beyond the scope of our study, we adopted a predetermined minimum acceptable ELS of  $10^{-7}$  in our model. Subsequently, we computed the minimum mean time between failures (MTBF) as a measure to evaluate the PER.

$$ELS_g = \frac{1}{MTBF} \times N_e \times P_f \quad (1)$$

where  $ELS_g$  is defined as the number of the ground fatalities per flight hour.  $N_e$  is the number of people that may be impacted by the debris or body of the UAV. It is a function of population density and the area exposed to the crash.  $P_f$  represents the probability of the individual suffering fatal injuries caused by the crash. It depends on the kinetic energy of the crashed UAV at the impact point and the sheltering factor.

More details of the two main components of the model are given in Sections 2.3.1 and 2.3.2.

#### 2.3.1. Number of People Exposed to the Crash

In order to more accurately assess the number of people exposed to the crash on the ground, it is essential to evaluate the population distribution and the geometric area of the UAV crash (critical area, CA). Urban population distribution is a parameter that is closely coupled with land use type [37]; the details are described in Section 2.2.2. With regard to the CA model, the JARUS model combines the RTI (Research Triangle Institute) [38] and NAWCAD (Naval Air Warfare Center Aircraft Division) [39] models and uses as few parameters as possible to analyze the CA of the UAV (Figure 5).

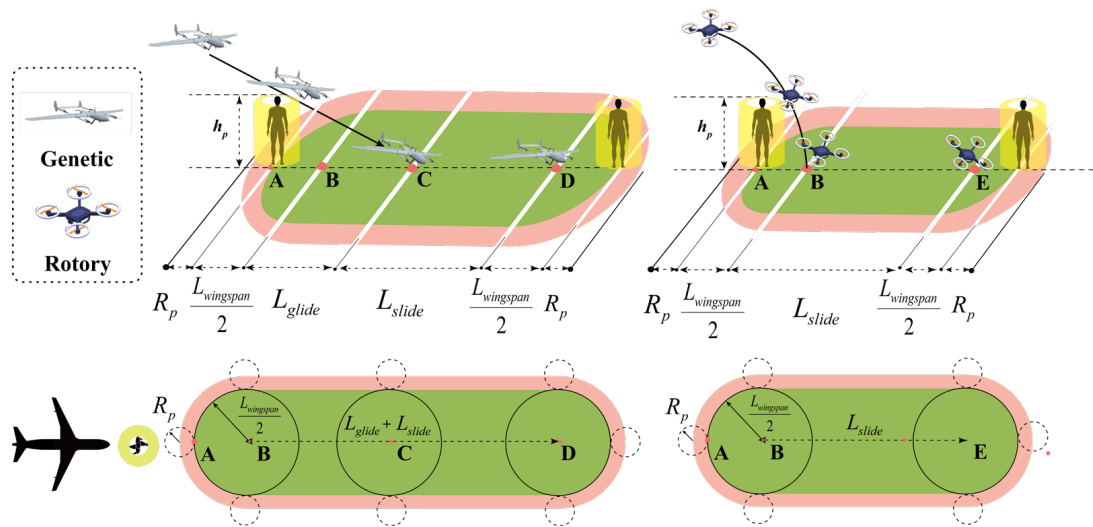


**Figure 5.** Critical area assessment model of unmanned aerial vehicle crash for generic and rotary types.

In Figure 5, the left and right sides correspond to the ground impact process for two types of UAVs. For the generic type, the length of the projection of its critical area in the horizontal plane consists of glide (where the aircraft is still airborne) and slide (where the aircraft is moving on the ground) distance. Moreover, due to the special aerodynamic properties of rotary UAVs, the glide distance will also be zero.

As given in Figure 5,  $R_p$  is the safe buffer zone of an average standing person ( $h_p = 1.75$  m) and  $L_{wingspan}/2$  is the maximum radius of the UAV dimension. A and C in Figure 5 depict two positions of a circularized flat piece, A when it is  $h_p$  feet above ground and C at impact. The glide distance (AC) is given as.

$$v_{horizontal} = v_{impact} \cos \theta \quad (2)$$

$$d_{glide} = \frac{h_p}{\tan \theta} \quad (3)$$

When a UAV collides with the ground in a vertical direction, i.e.,  $\theta = 90$  deg, the glide distance  $d_{glide}$  will be zero. However, in practical collision scenarios, such an occurrence is rare. Therefore, the glide distance is a parameter that is influenced by the height of the human and the angle of impact. In addition, the combined radius considering the person's safe buffer is defined as

$$R_D = R_p + \frac{L_{wingspan}}{2} \quad (4)$$

The part from C to D represents the sliding aircraft slowing down to a velocity at which the kinetic energy is no longer lethal. The maximum non-lethal kinetic energy is  $K_{non-lethal}$ , which gives the sliding aircraft a maximum non-lethal speed of

$$v_{non-lethal} = \sqrt{\frac{2K_{non-lethal}}{m}} \quad (5)$$

where  $m$  is the mass (this study uses the maximum takeoff mass for conservative estimation) of the UAV, assuming  $-C_g g$  represents the acceleration experienced by the aircraft during the slide process.  $C_g$  is the friction coefficient associated with the materials between the aircraft and the ground. The reduced residual horizontal speed is given by multiplication

with the coefficient of restitution  $e$ . Therefore, the time from impact to reaching non-fatal velocity is

$$t_{safe} = \frac{v_{non-lethal} - ev_{horizontal}}{-C_g g} \quad (6)$$

If  $t_{safe}$  becomes negative (which will happen if the horizontal impact speed is less than the maximum non-lethal speed in Equation (10)), it is set to zero. The slide distance with reduction during the time  $t_{safe}$  is

$$d_{slide, reduced} = ev_{horizontal} t_{safe} - \frac{1}{2} C_g g t_{safe}^2 \quad (7)$$

With the combination of glide and slide, the critical area of the JARUS model can be estimated with the following equation:

$$A_c = 2R_D(d_{glide} + d_{slide, reduced}) + \pi R_D^2 \quad (8)$$

Therefore, we used the JARUS model [16] and the land use type-based population distribution model to assess the number of people exposed to the crash in a risk map grid, which can be defined by Equation (1).

$$N_{exposed_i} = \sigma \times A_{critical} \times \frac{N_{grid} \times w_{landuse_i}}{A_{landuse_i}}, i = 1, 2, \dots, n \quad (9)$$

where  $N_{exposed_i}$  is defined as an estimation of the number of people exposed to an uncontrolled failure in the land use type  $i$ .  $\sigma$  is the estimated bias that in a critical area is assessed with the wind effect and the number of fragments. Based on the technical reports from the FAA [40],  $\sigma = 1.3$ .  $A_{critical}$  is the critical area in the JARUS model (illustrated in Figure 5 and calculated by Equations (3)–(9)).  $N_{grid}$  is the number of people in the risk map grid unit.  $w_{landuse_i}$  is the population distribution weighted coefficient of land use type  $i$ .  $A_{landuse_i}$  is the area of land use type  $i$  within the risk map grid unit.

### 2.3.2. Probability of Fatality

Previous research has employed parametric models to examine the risk of injury and fatalities. Two established indicators used to quantify head injuries from impact are the head injury criterion (HIC) and the Abbreviated Injury Scale (AIS) [21]. However, crashes caused by operating in urban areas do not necessarily cause direct damage; for instance, trees and buildings may provide shelter and thus increase the chances of survival. A drawback of the above model is that it is difficult to adjust it to take the sheltering effect into account. Dalamagkidis, Valavanis, and Piegl [11] proposed a model to assess the probability of fatality as a function of kinetic energy at impact that also takes into account sheltering and the correction factor  $k$  to improve the estimates for kinetic energy. This model is given by:

$$P_{fatality} = \frac{1 - k}{1 - 2k + \sqrt{\frac{\alpha}{\beta}} \left( \frac{\beta}{E_{impact}} \right)^{\frac{3}{P_s}}}, k = \min \left\{ 1, \left( \frac{\beta}{E_{impact}} \right)^{\frac{3}{P_s}} \right\} \quad (10)$$

where  $P_s$  represents the shelter factor, whose value is in the range of  $(0, \infty)$ . The higher values imply a better sheltering effect and a lower probability of fatality for the same kinetic energy.  $k$  is a correction factor used to improve the estimates provided for low kinetic energy. Parameter  $\alpha$  refers to the impact energy required for a 50% probability of death when  $P_s$  equals 6. Parameter  $\beta$  corresponds to the impact energy required to cause death

when  $P_s$  reaches zero. Based on the fatality limit defined in technical reports [41],  $\beta = 34$ ].  $E_{impact}$  is the kinetic energy at impact, computed as:

$$E_{impact} = \frac{1}{2}mv_{impact}^2 \quad (11)$$

where  $m$  is defined in Equation (5) and  $v_{impact}$  is the impact velocity at crash.

#### 2.4. Statistical Methods

First, we employed global spatial autocorrelation analysis to examine the overall correlation and variations of population exposure risk (PER) in the study area. Subsequently, local spatial autocorrelation analysis was conducted to identify cluster patterns of PER. To investigate the spatial dependence between PER and other urban geographical features, we utilized global bivariate Moran's I. This measure assesses the spatial correlation between the population and PER across the entire study area. The calculation of Bivariate Moran's I necessitates the use of spatial weight matrices, which represent the spatial relationships between the locations where the two variables are measured. In our study, we employed a spatial weight matrix based on queen contiguity with a first-order neighbor defined in a  $3 \times 3$  matrix. Bivariate Moran's I ranges from  $-1$  to  $1$ , with values close to  $1$  indicating strong positive spatial association, values close to  $-1$  indicating strong negative spatial association, and values close to  $0$  indicating random or weak spatial association. Permutation tests were conducted with 999 permutations to assess the statistical significance of bivariate Moran's I (assigned at  $p < 0.05$ ). Additionally, a Kruskal–Wallis analysis was performed to identify significant differences in PER among different urban functional areas (assigned at  $p < 0.05$ ). The relevant statistical analyses were conducted using the `scipy` and `pysal` packages in Python 3.8.

### 3. Results

#### 3.1. Assessing the Critical Area of UAV Crash

According to the estimation method in Section 2.3.2, the critical area is mainly determined by the weight and size of the UAV, the height and buffer radius of the ground person, the friction, and the angle and velocity at the impact point on the ground. In this study, the critical area was estimated using the iso-parametric method described in SORA, with impact angles and velocities ranging from a set minimum to maximum for both generic and rotary UAVs. The weight of the UAVs was estimated from the maximum takeoff weight listed in Table 2, with the height of the ground person assumed to be 1.75 m and the risk buffer radius set to 1 m. The friction coefficients were set to 0.6 and 0.9 for the generic and rotary UAVs, respectively, based on their material and shape. The results of this estimation are displayed in two-dimensional plots of critical area as a function of impact angle and velocity, with separate plots for each type of UAV, as shown in Figure 6.

**Table 2.** UAV parameters for population exposure risk analysis.

Type	Name	Wingspan (mm)	Length (mm)	MTOM (kg)	Speed (m/s)
Generic	ZhihangV330	3300	1650	15	25
Rotary	DJI Phantom 4 Pro	350	350	1.375	20

As depicted in Figure 6, the horizontal axis of the plots represents the impact angle and the vertical axis represents the velocity, with colors indicating the estimated impact area based on the model. Contours outlining typical critical areas are also added to the plot. A pattern is observed between the critical area and two factors—impact angle and velocity—for both experimental UAVs. As the impact angle increased, the effect of impact velocity on critical area decreased, as evidenced by the white contour line appearing to drop vertically when impact angle and velocity are small. This is due to an increase in impact angle, resulting in a decrease in horizontal velocity and a reduction in slide area,

leading to the critical area being primarily influenced by the glide. The generic UAV, due to its greater weight and shape, had a larger critical area compared to the rotary UAV.

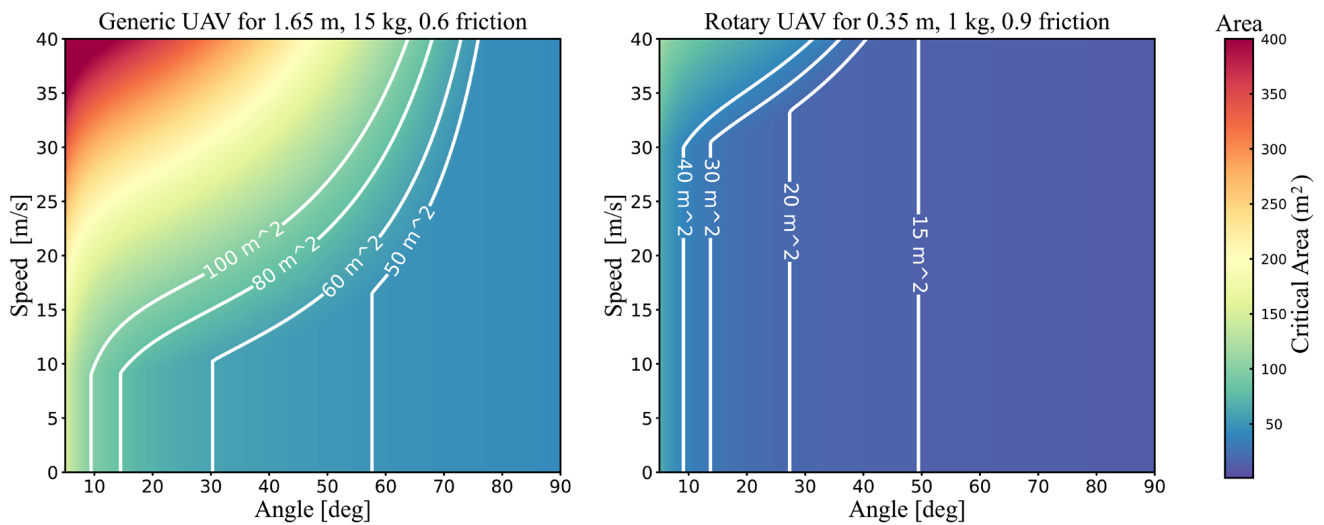


**Figure 6.** Isoparametric 2-D plot of critical area for various impact angle and velocities.

The above results had a similar pattern to the weight-based approach and the aircraft type-based study [15]. When data were collected from an actual accident or experimental simulation [24], the critical area did indicate a good fit based on vehicle weight. The difference in the two-dimensional probability density estimates of crash location between fixed-wing and multi-rotor aircraft further supports this [13]. However, it should be noted that using only the shape and mass of a UAV as the basis for risk classification and management is insufficient, as there are multiple factors that influence the ground kinetic energy. Therefore, it is necessary to conduct risk assessment for different types of UAVs based on specific operational scenarios and UAV specifications. In considering the uncertainties inherent in risk analysis, it is crucial to identify any sources of bias in order to estimate the true mean rather than a biased estimate. Determining these biases is a challenging task that often requires comparisons to empirical data or model results. Based on the above study and the FAA technical report, we added bias parameters (in Equation (9)) to estimate the critical area considering the dominant uncertainty sources, which be considered a constant with a value of 1.4.

### 3.2. Population Exposure Risk Characterization

Due to the inherent difficulties in quantifying failure rates of different UAV types operating in diverse regions, we adopted a substitution approach to assess the associated risks. Specifically, we employed a fixed acceptable safety level of  $10^{-7}$  within our model and calculated the MTBF for each urban grid cell. A longer MTBF, indicating a lower required failure rate, implies a higher risk of population exposure in the area. This highlights the imperative for implementing more stringent UAV safety management measures in the region. Utilizing the relevant parameters, we computed the risk values for each grid cell within the study area, which were subsequently visualized geographically in Figure 7. To facilitate a more comprehensive comparison, we present the minimum acceptable MTBF for the two UAV categories from three different perspectives: city-wide, regional, and micro-regional. To ensure consistency in our descriptions, we refer to the average failure rate times at acceptable equivalent safety levels as the population exposure risk (PER) in the subsequent sections of this paper.

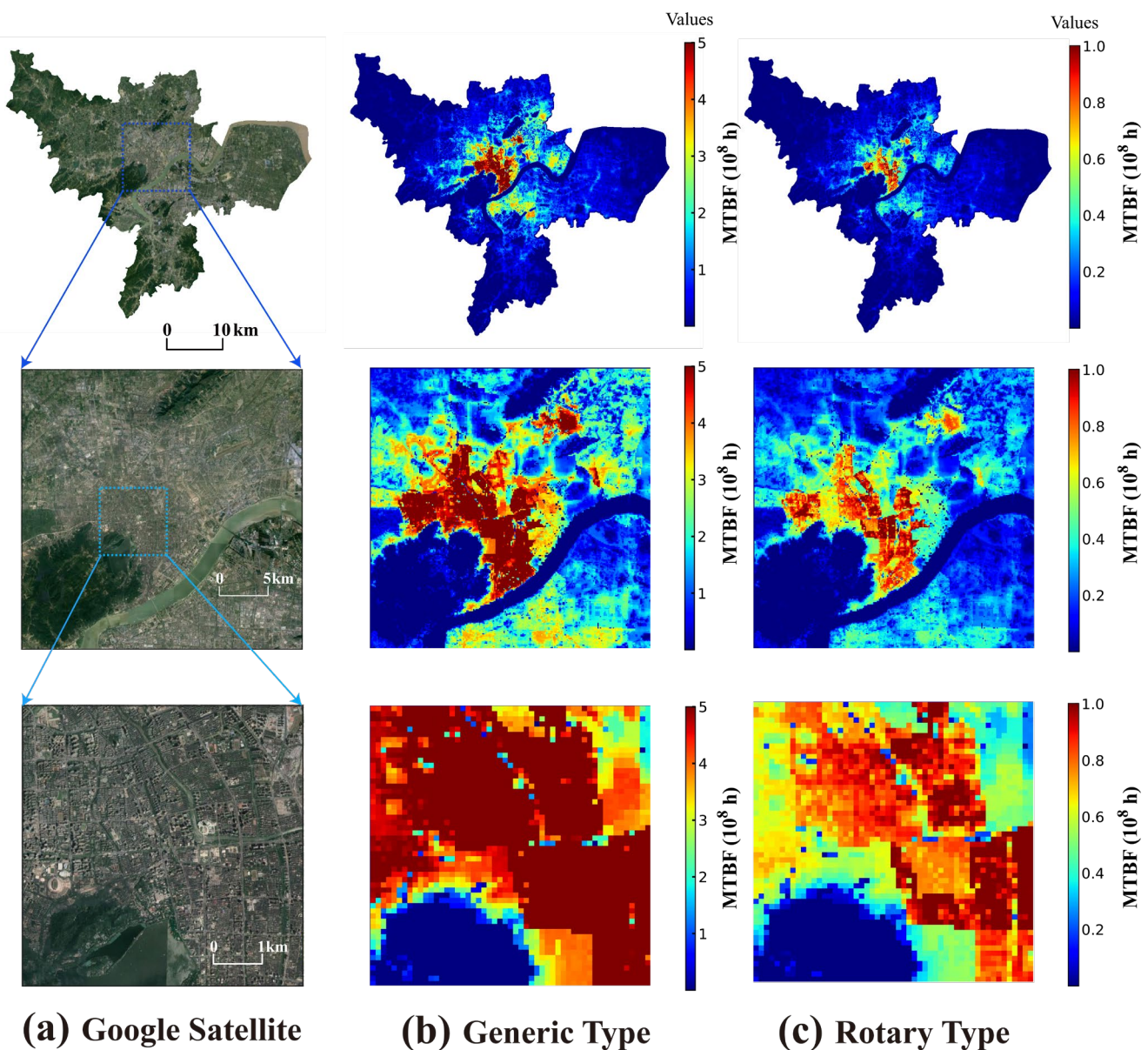


**Figure 7.** The spatial distribution of the minimum required mean time between failure (MTBF) for two types of UAVs at different scales of acceptable risk levels in urban areas of Hangzhou: (a) Google satellite data; (b) minimum required MTBF map of generic-type UAV; (c) minimum required MTBF map of rotary-type UAV.

The population exposure risk demonstrated spatial heterogeneity for both generic and rotary UAVs, with higher PER values observed in central urban areas, whereas relatively lower PER values were found in the eastern and western regions. Noteworthy similarities can be observed in the clustering patterns of PER and population density across various scales. To confirm this spatial correlation, a global bivariate Moran's I analysis was conducted, revealing Moran's I values of 0.83 ( $p < 0.01$ ) and 0.86 ( $p < 0.01$ ) for the population exposure risk of rotary and generic UAVs, respectively, when considered alongside population density. These results indicate that regions with higher population density tend to exhibit an increased population exposure risk not only within the region itself but also in the surrounding areas. Statistical calculations were performed to determine the mean and maximum PER values for the generic and rotary UAV types. The generic UAV type demonstrated a mean PER of  $6.48 \times 10^7$ , with a maximum value of  $9.04 \times 10^8$ , whereas the rotary UAV type exhibited a mean PER of  $8.67 \times 10^6$ , with a maximum value of  $1.22 \times 10^8$ .

Examining the overall spatial pattern, it is evident that the PER values for the generic UAV type exceeded our predefined acceptable range in almost all populated areas of the study region. Conversely, the PER values for the rotary UAV type surpassed the acceptable range solely within the core urban area. Further analysis at finer scales revealed that high PER hotspots were concentrated in central urban areas characterized by a high population density. In contrast, low PER areas were predominantly located in the northwestern and southeastern parts of the study region, as well as in the central section of the Qiantang River. Through additional examination, it became apparent that this clustering of PER values primarily stemmed from the intense urbanization observed within the inner city, resulting in higher population density and mobility. Notably, these areas possess a greater capacity for providing shelter.

To further explore the characteristics of PER, we conducted an analysis to examine the differentiation of PER across different urban functional areas. It is important to note that we excluded airport facilities from our analysis, as they are designated as no-fly zones for UAVs. In Figure 8a,b, we present the different urban functional areas from a general and a local perspective, respectively. The “1-Other” functional area encompasses land cover types such as arable land, forest, grassland, scrub, wetland, water, and bare ground, excluding impervious surfaces. Figure 8c,d display the PER box line diagrams for the two types of UAVs in the different urban functional areas, with the solid lines in the boxes representing the 25th percentile, median, and 75th percentile.

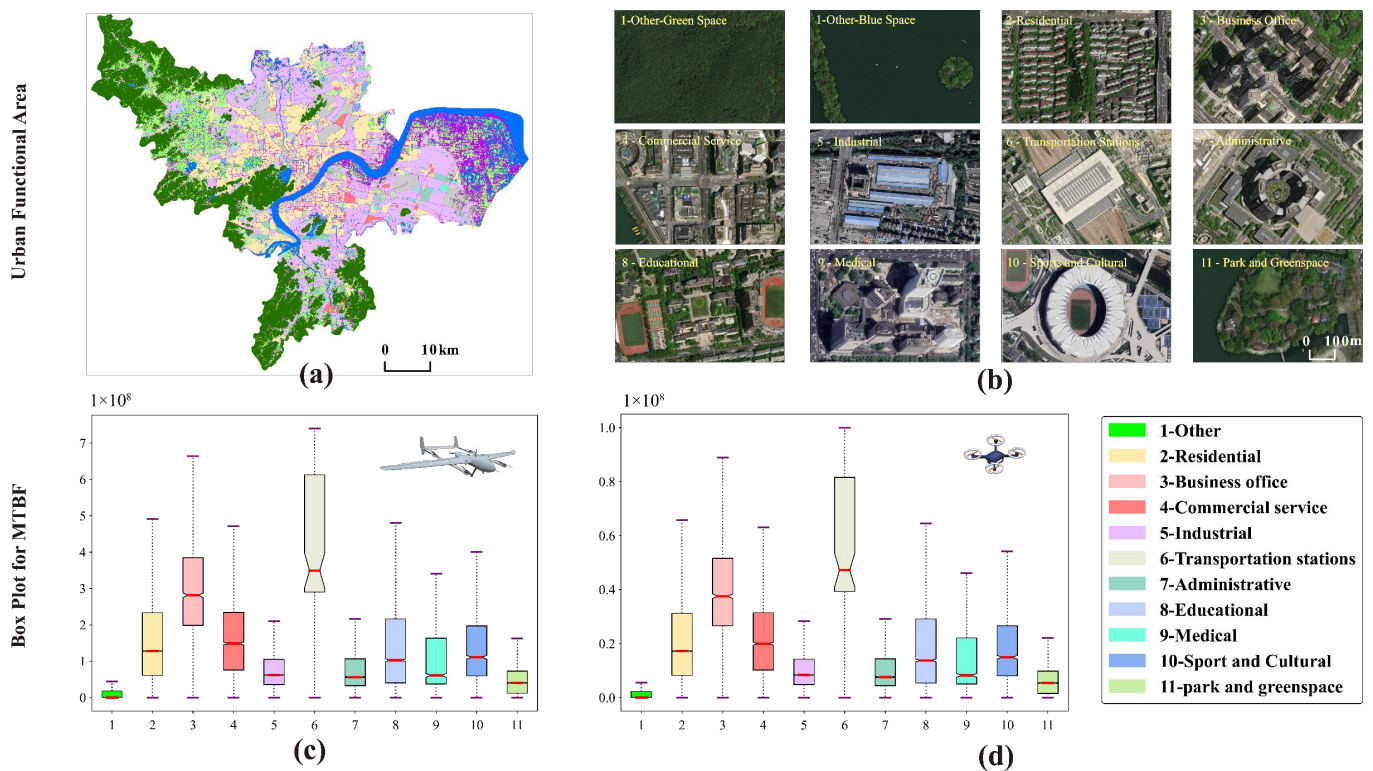


**Figure 8.** Comparison of population number and population exposure risk among the grid units at each functional area in Hangzhou. (a) Urban land use and functional area from a global perspective and (b) from a local perspective; (c) population exposure risk for generic type and (d) for rotary type. The colors and numbers in the legends at the lower right corner correspond to the different functional areas depicted in subfigures (a–d).

To compare the PERs of the different zones, we employed a non-parametric Kruskal–Wallis test. Our results revealed a significant difference ( $p < 0.01$ ) in PER between rotary and regular drones across various urban functional areas. Figure 8b,c present zonal statistics of PER levels for generic and rotary UAV operations in various urban functional areas.

Although both UAV types exhibited similar risk variations across these areas, the risk associated with the generic type was approximately six times higher compared to the rotary type. These discrepancies can be attributed to the distinct physical properties and ground impact process inherent to each UAV type. Notably, high-risk areas for both types of drones were predominantly concentrated in transport stations, followed by business offices, commercial service areas, residential areas, educational institutions, sports and cultural facilities, medical facilities, administrative centers, and industrial areas. In contrast, areas with parks and other natural elements had relatively lower risk. These findings are in line with our population size model.

### 3.3. Exploring the Risk and Disparities Based on Different Spatial Units

To assess the impact of using different spatial units for risk assessment, we compared the risk of population exposure for both UAV types at the street-level census spatial cells and 100 m spatial grids. Figure 9a,b illustrate a three-dimensional visualization of PER for a generic-type UAV under the two spatial units, utilizing the three-scale perspective shown in Figure 7. The results revealed a more pronounced averaging effect in the census faceted cells, whereas the 100 m regular grids provided finer spatial detail as the scale became finer. To compare the risk quantification values between the two spatial units, we utilized spatial operations to subtract the quantification values of the census cells from those of the regular grids.

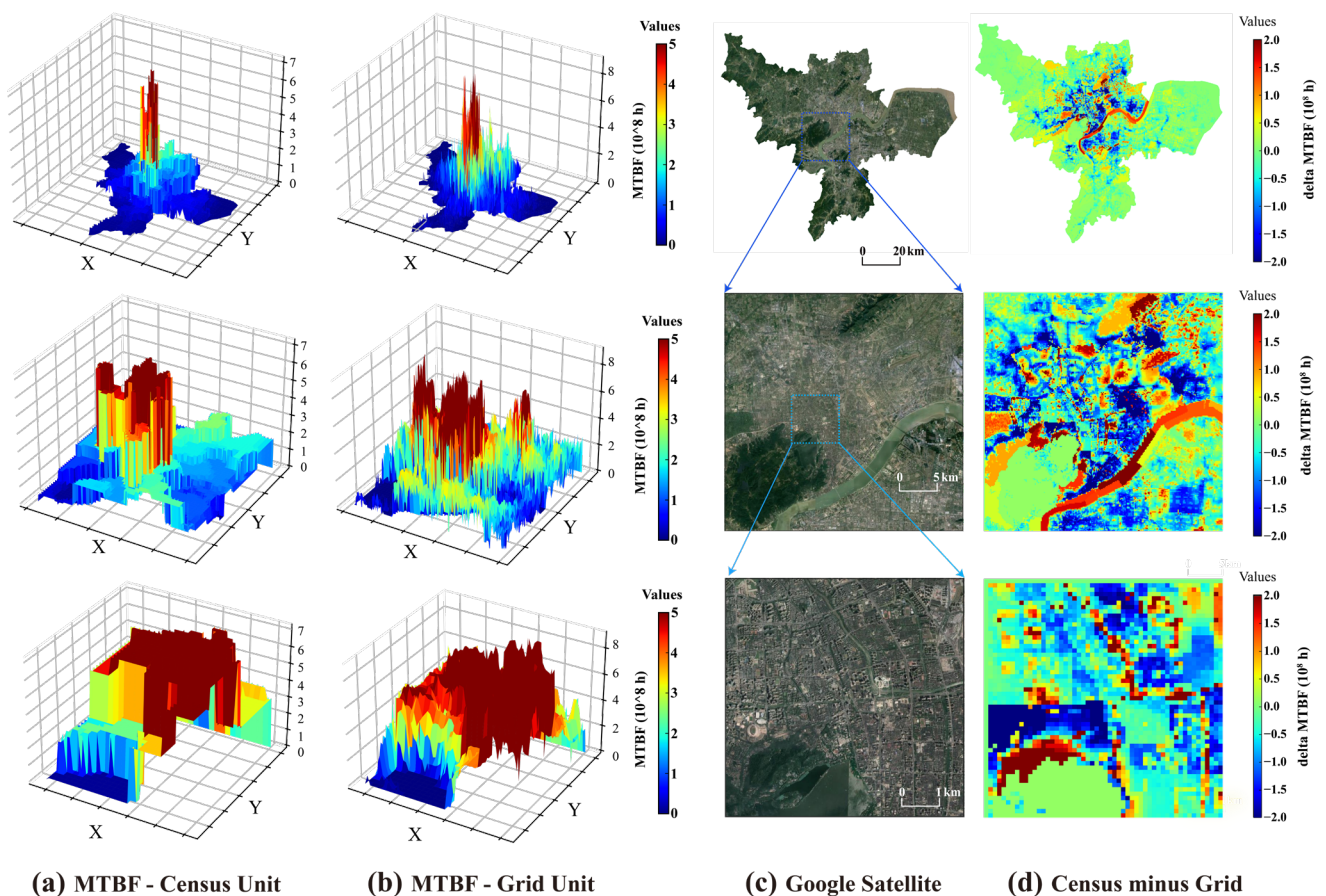


**Figure 9.** Spatial distribution of population exposure risks and assessment errors for census units and 100 m regular grids. (a,b) Three-dimensional visualization of PER for generic-type UAV under the census and grid spatial units; (c) Google Satellite; (d) spatial error map: census unit minus grid cell space.

The resulting spatial distribution of risk deviations, depicted in Figure 9d, exhibited a core–edge structure in urban spatial space. In urban fringe areas characterized by lower

population density, the use of spatial units had a smaller impact on the accuracy of risk assessment, resulting in fewer errors. However, in densely populated areas located in urban centers, errors in risk assessment due to the choice of spatial units became more evident. More specifically, the utilization of census units for risk assessment in central urban areas featuring natural elements like rivers and grasslands tended to result in an overestimation of risk, with values reaching up to  $4 \times 10^8$ . Conversely, in densely populated and built-up areas, the use of census units led to an underestimation of risk, with values reaching up to  $2 \times 10^8$ .

The univariate local Moran's index was used to further analyze the risk of population exposure and the spatial aggregation of risk errors. According to the cluster and outlier analysis at the 1% significance level, the cluster distribution of the generic-type UAV (first row of Figure 10) was almost identical to that of the rotary type (second row of Figure 10). The figure visualizes the spatial clustering of population exposure risk within the study area of Hangzhou. Most areas fell into HH and LL clusters, with a few areas in L-H and H-L outliers. These patterns provide evidence of the positive spatial autocorrelation that exists within the study area. For both scales of PER, areas characterized by the HH clusters were concentrated in the urban core, whereas the LL clusters showed a clear pattern of distribution in the urban periphery. These observations are in line with our previous findings in Section 3.1.

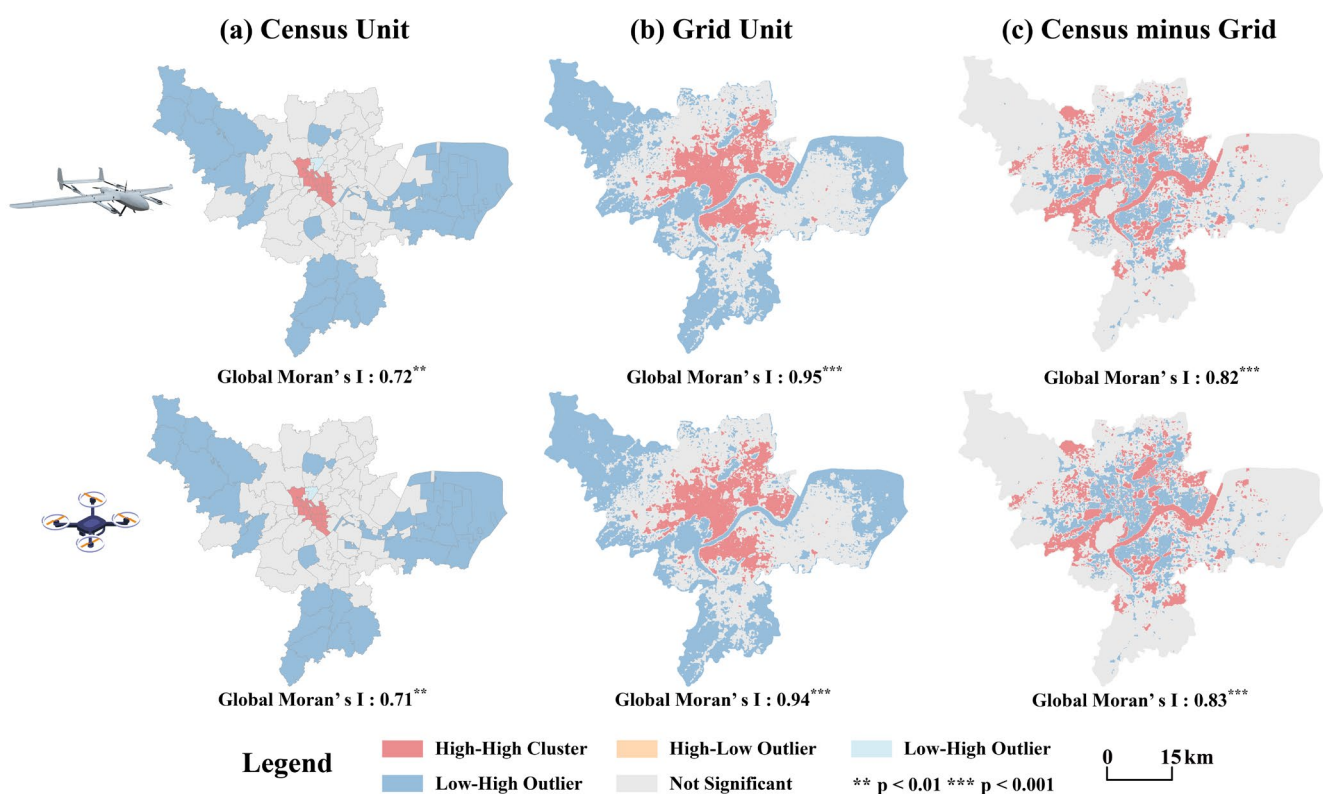


**Figure 10.** The global and local Moran's index in the study area. The two rows correspond to two types of drones, generic and rotary wing. The three columns correspond to the census unit, the regular grid cell, and their bias.

Furthermore, when scrutinizing the disparities in PER across the two scales, it became evident that the HH and LL aggregation types were significantly prevalent within the urban core. Remarkably, both HH and LL types of clusters correspond to the areas where the census units exhibited a tendency to overestimate and underestimate risk aggregation, respectively. In culmination, these results reflect the existence of positive spatial autocorre-

lation of both population exposure risk and risk bias within the confines of the Hangzhou study area.

## 4. Discussion

### 4.1. Population Exposure Risk Characterization

UAS will need to satisfy public safety standards. Level of risk is one of the commonalities between most global certification authorities [27]. The risk level associated with these platforms varies depending on their size and speed. As UAV increase in size and weight, government regulations become more stringent, specifying the purpose of operations and the level of training required for operators [42]. Certification authorities currently face a deficiency in comprehensive analysis of operational data and reports on unsafe events related to civil UAVs. This limitation can impede the decision-making process, resulting in delays or biased results. Furthermore, many existing studies have employed simplistic census units for risk assessment in urban areas, leading to distorted estimations [27]. This discrepancy exacerbates the conflict between the demand for UAV operations in densely populated regions and the inaccurate quantification of risk assessment in such areas. In light of the relevant findings presented in this study, we contend that meticulous attention should be paid to airworthiness certification and risk management when planning UAV operations in urban areas. Tailored test and evaluation methods for each UAV type and a deeper understanding of the capabilities and limitations of different UAVs are essential in order to provide more accurate guidance for the sustainable management of aerospace. Furthermore, assessment and certification processes must be tailored to different cities within the same country or even distinct areas within a single city. Concerning the utilization of spatial population data for assessments, it is recommended to employ high-precision population grid data for densely populated areas. However, the criteria for delineating sparse and dense populations may vary from country to country, making it challenging to establish a uniform standard. It is advisable to characterize the intensity of population activity in conjunction with the extent of urban built-up areas or the proportion of urban impervious surfaces.

The spatial gridded model proposed in this study, which subdivides the urban area into unique cells corresponding to MTBF, can serve as a foundation for airworthiness certification and route planning for UAVs in various urban areas. To establish a systematic process, it is recommended to initiate pilot applications in low-risk scenarios within urban areas, prioritizing locations abundant in natural geographical elements such as rivers, woods, and other similar features. This strategy facilitates the construction of a robust framework for risk assessment in typical scenarios. With the accumulation of operational experience, standardized scenarios (STS) can be systematically developed, ensuring a structured and iterative process. Furthermore, this approach can be expanded in the future to encompass a diverse range of standard scenarios tailored to different urban functional areas and application scenarios. The adoption of such an approach significantly simplifies the assessment and supervision process, providing a more efficient and comprehensive framework.

### 4.2. Model Advantages and Limitations

This study indicates that grid-based risk map analysis is a powerful method to analyze the spatial pattern and hotspots of PER, which could be used to detect the high PER areas in a city. Multi-source big data, such as high spatial resolution population grid data, land cover/land use data, and city-scale building data, were used as the risk element layers in this study to evaluate the PER of UAS operations. In the case of population, the most important component of population exposure risk, we divided the geographic space into a homogeneous grid, and within each grid the population distribution was further subdivided according to various land cover types and buildings, which reduced overly conservative estimates due to uniform population distribution. In addition, the grid can be further appended with all kinds of attribute information, including high spatial and temporal resolution geo-fencing and other information. The grid unit can be integrated

with various risk assessment models, which can eventually be applied to path planning, air traffic management, airspace resource management, etc. These assessed PER maps and hotspots are particularly important for government managers or urban planners to mitigate and reduce exposure risks of small UAS operations in urban low-airspace environments. In addition to the advantages of the PER analysis of small UAVs operated in the urban environment described above, this study has limitations.

Firstly, uncertainty concerning the population mobility and spatial pattern can be attributed to numerical estimates in parameterizations and mismatches in spatial resolution of various types of geographical data. Specifically, although we used higher-resolution data and weighting factors for the population estimates, in practice, spatial variation in population distribution is not static, with hourly, daily, weekly, and seasonal changes. Such spatio-temporal effects have a major role in determining the variations in exposure, especially in a populated area. It would be valuable to investigate and quantify these weight factors using big data such as cellular networks and smart-ID data in future surveys.

Secondly, the critical area model in PERM consists of a rectangle as wide as the combination of wingspan and person buffer and as long as the glide and slide distance. However, there can be significant differences in the calculation of critical area in built-up urban areas and open areas. For example, in areas with high levels of urban build-up, UAVs may crash on buildings before falling to human height, resulting in debris that may affect even larger physical areas.

Last but not least, the estimation of UAS failure is fixed in this study, but UAS failure is much more complicated when combined with weather, electromagnetic environment, and crowded buildings [5,23]. Furthermore, we did not consider that some UAS might have recovery measures to address these failures (e.g., use of redundant systems). Although a higher level of accident data and structural/functional information of hardware would increase the potential sources of data available for the PER model, reliability data at this level may not be accessible or may come at a significant monetary cost [11].

## 5. Conclusions

The present study underscores the significance of conducting quantitative risk assessment for sustainable urban air traffic management, particularly in the context of integrating UAS into national airspace. To this end, a geographic data-driven framework was developed to evaluate the population exposure risk (PER) associated with unmanned aerial system (UAS) operations. The proposed framework adopts a human-centric approach by generating a grid-based risk map to estimate PER within a city-scale area, taking into account population size, crash area, and ground sensitivity to UAS crashes. The framework was applied to two popular types of UAVs in Hangzhou, allowing for an investigation of how UAV variables, shelter factors, and population characteristics influence PER in different functional areas of the city. A comparison with census spatial units was also conducted. The key findings of our study are as follows:

- (1) Significant variations in PER were observed among different types of UAVs operating in urban low airspace, attributable to their varying shapes, weights, and performance characteristics. In central urban areas, the average MTBF was found to be  $10^8$  orders of magnitude, indicating the need for stringent hardware and software management requirements to maintain an acceptable level of risk.
- (2) Spatial heterogeneity and multiscale effects were identified in the spatial pattern of PER in urban areas, consistent with the distribution of the population. Areas with high population mobility, such as transport hubs, commercial services, and residential and business areas, exhibited higher PER. Conversely, natural land uses, such as vegetation, water bodies, and croplands, generally presented lower PER levels.
- (3) The utilization of census units in risk assessment within urban areas presents a potential for biased estimation, particularly in regions exhibiting substantial levels of urban build-up. Specifically, higher degrees of urban build-up are prone to the underestimation of risk, whereas lower degrees can engender an overestimation. This

highlights the significance of considering suitable spatial units to ensure accurate risk quantification and assessment in areas with varying levels of urban development.

In future research, several directions can be pursued. Firstly, the PER model should be expanded to encompass a wider range of UAV types and operation scenarios and incorporate real-world accident data to facilitate more realistic and practical urban air mobility management decisions. Secondly, the integrated modeling framework can be further extended to consider vulnerability to UAS crashes based on different regions and age groups. Additionally, future work should explore the utilization of high spatio-temporal resolution population distribution data instead of static historical data, enabling more accurate and multi-scale estimation of PER.

**Author Contributions:** Conceptualization, H.H. and X.L.; methodology, H.H., C.X. and H.Y. (Huanyin Yue); software, H.H., H.Y. (Huanyin Yue) and C.X.; data curation, H.Y. (Huping Ye) and H.H.; writing—original draft preparation, H.H. and C.X.; writing—review and editing, H.Y. (Huping Ye) and X.L.; supervision, H.Y. (Huping Ye); funding acquisition, X.L. All authors have read and agreed to the published version of the manuscript.

**Funding:** This study was partly supported by the National Key R&D Program of China (Project No. 2022YFC3800700), the Strategic Priority Research Program of the Chinese Academy of Sciences (No. XDA28050200, XDA19040104), the National Natural Science Foundation of China (No. 41971359).

**Data Availability Statement:** The codes used in this study are available upon request to the corresponding author.

**Conflicts of Interest:** The authors declare no conflict of interest.

## Abbreviations

AIS	Abbreviated Injury Scale
CA	Critical area
DEM	Digital elevation model
ELS	Equivalent level of safety
FAA	Federal Aviation Administration
FROM-GLC	Finer Resolution Observation and Monitoring of Global Land Cover
GIS	Geographic Information System
GPW	Gridded population of the world
GRM	Ground risk model
HIC	Head injury criterion
JARUS	Joint Authorities for Rulemaking on Unmanned Systems
MTBF	Mean time between failure
NTSB	National Transportation Safety Board
NAWCAD	Naval Air Warfare Center Aircraft Division
PER	Population exposure risk
PERM	Population exposure risk model
RTI	Research Triangle Institute
SORA	Specific Operations Risk Assessment
UAS	Unmanned aerial system
UAV	Unmanned aerial vehicle

## References

1. Yao, H.; Qin, R.; Chen, X. Unmanned Aerial Vehicle for Remote Sensing Applications—A Review. *Remote Sens.* **2019**, *11*, 1443. [[CrossRef](#)]
2. Rejeb, A.; Rejeb, K.; Simske, S.J.; Treiblmaier, H. Drones for supply chain management and logistics: A review and research agenda. *Int. J. Logist. Res. Appl.* **2023**, *26*, 708–731. [[CrossRef](#)]
3. Floreano, D.; Wood, R.J. Science, technology and the future of small autonomous drones. *Nature* **2015**, *521*, 460–466. [[CrossRef](#)] [[PubMed](#)]
4. Mohamed, N.; Al-Jaroodi, J.; Jawhar, I.; Idries, A.; Mohammed, F. Unmanned aerial vehicles applications in future smart cities. *Technol. Forecast. Soc. Chang.* **2020**, *153*, 119293. [[CrossRef](#)]

5. Washington, A.; Clothier, R.A.; Silva, J. A review of unmanned aircraft system ground risk models. *Prog. Aerosp. Sci.* **2017**, *95*, 24–44. [[CrossRef](#)]
6. McCarthy, T.; Pforte, L.; Burke, R. Fundamental Elements of an Urban UTM. *Aerospace* **2020**, *7*, 85. [[CrossRef](#)]
7. Ma, T.; Zhou, C.H.; Pei, T.; Haynie, S.; Fan, J.F. Quantitative estimation of urbanization dynamics using time series of DMSP/OLS nighttime light data: A comparative case study from China's cities. *Remote Sens. Environ.* **2012**, *124*, 99–107. [[CrossRef](#)]
8. Zhou, G.; Li, C.; Liu, Y.; Zhang, J. Complexity of Functional Urban Spaces Evolution in Different Aspects: Based on Urban Land Use Conversion. *Complexity* **2020**, *2020*, 9741203. [[CrossRef](#)]
9. Xu, C.; Liao, X.; Tan, J.; Ye, H.; Lu, H. Recent Research Progress of Unmanned Aerial Vehicle Regulation Policies and Technologies in Urban Low Altitude. *IEEE Access* **2020**, *8*, 74175–74194. [[CrossRef](#)]
10. Federal Aviation Administration. *System Safety Handbook*; US Department of Transportation, Federal Aviation Administration: Washington, DC, USA, 2000.
11. Dalamagkidis, K.; Valavanis, K.P.; Piegel, L.A. *On Integrating Unmanned Aircraft Systems into the National Airspace System: Issues, Challenges, Operational Restrictions, Certification, and Recommendations*, 2nd ed.; Springer Publishing Company, Incorporated: New York, NY, USA, 2013.
12. Lum, C.; Waggoner, B. *A Risk Based Paradigm and Model for Unmanned Aerial Systems in the National Airspace*; American Institute of Aeronautics and Astronautics: Orlando, FL, USA, 2011.
13. Primates, S.; Rizzo, A.; la Cour-Harbo, A. Ground Risk Map for Unmanned Aircraft in Urban Environments. *J. Intell. Robot. Syst.* **2019**, *97*, 489–509. [[CrossRef](#)]
14. Weibel, R.; Hansman, R.J. Safety Considerations for Operation of Different Classes of UAVs in the NAS. In Proceedings of the AIAA 3rd “Unmanned Unlimited” Technical Conference, Workshop and Exhibit, Chicago, IL, USA, 20–23 September 2004.
15. Zhang, X.; Liu, Y.; Zhang, Y.; Guan, X.; Delahaye, D.; Tang, L. Safety Assessment and Risk Estimation for Unmanned Aerial Vehicles Operating in National Airspace System. *J. Adv. Transp.* **2018**, *2018*, 4731585. [[CrossRef](#)]
16. Joint Authorities for Rulemaking of Unmanned Systems. JARUS Guidelines on Specific Operations Risk Assessment (SORA), Public Release Edition 2.0. 2023. Available online: [http://jarus-rpas.org/wp-content/uploads/2023/06/jar\\_09\\_doc\\_JARUS\\_SORA\\_Executive\\_Summary.pdf](http://jarus-rpas.org/wp-content/uploads/2023/06/jar_09_doc_JARUS_SORA_Executive_Summary.pdf) (accessed on 1 July 2023).
17. Cain, S.; Torens, C.; Volkert, A.; Juchmann, P.; Tomasello, F.; Natale, M.; Vreeken, J.; Birgelen, T.v.; Ribeiro, M.; Ellerbroek, J.; et al. Standards for UAS—Acceptable Means of Compliance for Low Risk SORA Operations. In Proceedings of the AIAA Scitech 2021 Forum, Virtual, 11–15 January 2021.
18. Blom, H.A.; Jiang, C.; Grimme, W.B.; Mitici, M.; Cheung, Y.S. Third party risk modelling of Unmanned Aircraft System operations, with application to parcel delivery service. *Reliab. Eng. Syst. Saf.* **2021**, *214*, 107788. [[CrossRef](#)]
19. Che Man, M.H.; Haoliang, H.; Low, K.H. Crash Area Estimation for Ground Risk of Small Unmanned Aerial Vehicles Due to Propulsion System Failures. In Proceedings of the AIAA SCITECH 2022 Forum, San Diego, CA, USA, 3–7 January 2022.
20. Melnyk, R.; Schrage, D.; Volovoi, V.; Jimenez, H. A third-party casualty risk model for unmanned aircraft system operations. *Reliab. Eng. Syst. Saf.* **2014**, *124*, 105–116. [[CrossRef](#)]
21. Koh, C.H.; Low, K.H.; Li, L.; Zhao, Y.; Deng, C.; Tan, S.K.; Chen, Y.; Yeap, B.C.; Li, X. Weight threshold estimation of falling UAVs (Unmanned Aerial Vehicles) based on impact energy. *Transp. Res. Part C Emerg. Technol.* **2018**, *93*, 228–255. [[CrossRef](#)]
22. Walker, R.; Clothier, R. Safety Risk Management of Unmanned Aircraft Systems. In *Handbook of Unmanned Aerial Vehicles*; Valavanis, K., Vachtsevanos, G., Eds.; Springer: Dordrecht, The Netherlands, 2015.
23. Han, P.; Yang, X.; Zhao, Y.; Guan, X.; Wang, S. Quantitative Ground Risk Assessment for Urban Logistical Unmanned Aerial Vehicle (UAV) Based on Bayesian Network. *Sustainability* **2022**, *14*, 5733. [[CrossRef](#)]
24. Kim, Y.; Bae, J. Risk-Based UAV Corridor Capacity Analysis above a Populated Area. *Drones* **2022**, *6*, 221. [[CrossRef](#)]
25. Pang, B.; Hu, X.; Dai, W.; Low, K.H. UAV path optimization with an integrated cost assessment model considering third-party risks in metropolitan environments. *Reliab. Eng. Syst. Saf.* **2022**, *222*, 108399. [[CrossRef](#)]
26. Ren, X.; Cheng, C. Model of Third-Party Risk Index for Unmanned Aerial Vehicle Delivery in Urban Environment. *Sustainability* **2020**, *12*, 8318. [[CrossRef](#)]
27. Wardrop, N.A.; Jochem, W.C.; Bird, T.J.; Chamberlain, H.R.; Clarke, D.; Kerr, D.; Bengtsson, L.; Juran, S.; Seaman, V.; Tatem, A.J. Spatially disaggregated population estimates in the absence of national population and housing census data. *Proc. Natl. Acad. Sci. USA* **2018**, *115*, 3529–3537. [[CrossRef](#)]
28. Yao, Y.; Liu, X.; Li, X.; Zhang, J.; Liang, Z.; Mai, K.; Zhang, Y. Mapping fine-scale population distributions at the building level by integrating multisource geospatial big data. *Int. J. Geogr. Inf. Sci.* **2017**, *31*, 1220–1244. [[CrossRef](#)]
29. Gong, P.; Chen, B.; Li, X.; Liu, H.; Wang, J.; Bai, Y.; Chen, J.; Chen, X.; Fang, L.; Feng, S.; et al. Mapping essential urban land use categories in China (EULUC-China): Preliminary results for 2018. *Sci. Bull.* **2020**, *65*, 182–187. [[CrossRef](#)]
30. Leyk, S.; Gaughan, A.E.; Adamo, S.B.; de Sherbinin, A.; Balk, D.; Freire, S.; Rose, A.; Stevens, F.R.; Blankespoor, B.; Frye, C.; et al. The spatial allocation of population: A review of large-scale gridded population data products and their fitness for use. *Earth Syst. Sci. Data* **2019**, *11*, 1385–1409. [[CrossRef](#)]
31. Doxsey-Whitfield, E.; MacManus, K.; Adamo, S.B.; Pistolesi, L.; Squires, J.; Borkovska, O.; Baptista, S.R. Taking Advantage of the Improved Availability of Census Data: A First Look at the Gridded Population of the World, Version 4. *Pap. Appl. Geogr.* **2015**, *1*, 226–234. [[CrossRef](#)]

32. Bright, E.A.; Coleman, P.R.; Dobson, J.E. LandScan: A Global Population Database for Estimating Populations at Risk. *Photogramm. Eng. Remote Sens.* **2000**, *66*, 849–858.
33. Tatem, A.J. WorldPop, open data for spatial demography. *Sci. Data* **2017**, *4*, 170004. [[CrossRef](#)] [[PubMed](#)]
34. Zhu, W.; Chen, J. The spatial analysis of digital economy and urban development: A case study in Hangzhou, China. *Cities* **2022**, *123*, 103563. [[CrossRef](#)]
35. Xu, C.; Liao, X.; Fei, Y. IEEE Standard Pioneered an It-Led Interdisciplinary Approach to Structure Low-Altitude Airspace for Uav Operations. *Sci. China Inf. Sci.* **2022**, *65*, 207201. [[CrossRef](#)]
36. Su, Y.; Xu, Y. Risk-Based Flight Planning and Management for Urban Air Mobility. In *AIAA AVIATION 2022 Forum*; American Institute of Aeronautics and Astronautics: Chicago, IL, USA, 2022. [[CrossRef](#)]
37. Tan, M.; Li, X.; Li, S.; Xin, L.; Wang, X.; Li, Q.; Li, W.; Li, Y.; Xiang, W. Modeling population density based on nighttime light images and land use data in China. *Appl. Geogr.* **2018**, *90*, 239–247. [[CrossRef](#)]
38. Montgomery, R.M. *Casualty Areas from Impacting Inert Debris for People in the Open*; Research Triangle Institute: Research Triangle Park, NC, USA, 1995.
39. Ball, J.A.; Knott, M.; Burke, D. *Crash Lethality Model*; Naval Air Warfare Center Aircraft Division: Patuxent River, MD, USA, 2012.
40. Associate Administrator for Commercial Space Transportation. *Flight Safety Analysis Handbook*. 2011. Available online: [https://www.faa.gov/about/office\\_org/headquarters\\_offices/ast/media/Flight\\_Safety\\_Analysis\\_Handbook\\_final\\_9\\_2011v1.pdf](https://www.faa.gov/about/office_org/headquarters_offices/ast/media/Flight_Safety_Analysis_Handbook_final_9_2011v1.pdf) (accessed on 1 July 2023).
41. Range Commanders Council Range Safety Group Risk Committee. *Common Risk Criteria Standards for National Test Ranges: Supplement*; US Army White Sands Missile Range: White Sands Missile Range, NM, USA, 2007.
42. Tepylo, N.; Straubinger, A.; Laliberte, J. Public perception of advanced aviation technologies: A review and roadmap to acceptance. *Prog. Aerosp. Sci.* **2023**, *138*, 100899. [[CrossRef](#)]

**Disclaimer/Publisher's Note:** The statements, opinions and data contained in all publications are solely those of the individual author(s) and contributor(s) and not of MDPI and/or the editor(s). MDPI and/or the editor(s) disclaim responsibility for any injury to people or property resulting from any ideas, methods, instructions or products referred to in the content.